

Geophysical Research Letters

RESEARCH LETTER

10.1029/2020GL087452

Key Points:

- Airborne UAVSAR interferometry elucidates local variations in magnitude and orientation of displacements at the Slumgullion landslide
- High-resolution LiDAR DEM reveals the landslide thickness at the emergent toe
- InSAR-measured landslide speed helps constrain the material viscosity (10^9 – $10^{11.5}$ Pa·s at the Slumgullion) based on Bingham plastic model

Supporting Information:

- Supporting Information S1

Correspondence to:

X. Hu,
xiehu@berkeley.edu

Citation:

Hu, X., & Bürgmann, R. (2020). Rheology of a debris slide from the joint analysis of UAVSAR and LiDAR data. *Geophysical Research Letters*, 47, e2020GL087452. <https://doi.org/10.1029/2020GL087452>

Received 9 FEB 2020

Accepted 5 APR 2020

Accepted article online 17 APR 2020

Rheology of a Debris Slide From the Joint Analysis of UAVSAR and LiDAR Data

Xie Hu¹  and Roland Bürgmann² 

¹Berkeley Seismological Laboratory, University of California, Berkeley, CA, USA, ²Department of Earth and Planetary Science, University of California, Berkeley, CA, USA

Abstract Landslide rheology governs the deformation and flow behavior of sliding masses. As rheology strongly varies as a function of the composition and environment of landslides, a wide range of viscosities have been suggested based on very limited experimental or observational constraints. Here, we introduce a novel method to quantify the landslide rheology from remote sensing data. We focus on an ideal natural laboratory, the Slumgullion landslide, Colorado, which has moved at tens of millimeters per day for centuries. A joint analysis of Uninhabited Aerial Vehicle Synthetic Aperture Radar (UAVSAR) Interferometric Synthetic Aperture Radar (InSAR)-derived surface displacements and Light Detection and Ranging (LiDAR) Digital Elevation Model (DEM)-derived landslide thickness at its frontal toe allows us to invert for the intrinsic viscosity (10^9 – $10^{11.5}$ Pa·s under different degrees of plasticity) based on the Bingham plastic model. Detailed displacement measurements also elucidate local variations in magnitude and orientation. Our method presents the capability of remote sensing data to understand the rheology of quasi-static debris slides in general.

Plain Language Summary Landslides are common geological hazards that may lead to casualties and damage. Landslides also present as a surface process that reshapes mountainous landscapes around the world. The soil and rock materials, water content, and the associated vegetation and organic matter contribute to a variety of landslide mechanical properties and rheology, which characterize the slide/flow approximation of the mass wasting process and thus the landslide speed. To date, the determination of the landslide rheology has mainly relied on analyzing samples in the lab. However, many landslides are inaccessible for sample collection, and the lab environment subject to isolated and small samples can hardly be compared to the intact landslide in nature. Taking advantage of high-resolution airborne remote sensing data sets at the Slumgullion debris slide in Colorado, we extract the landslide surface displacements and topography. Incorporating our observations, we consider a classic model in fluid mechanism to infer the rheological parameters. We also identify the spatiotemporally variable landslide movements. A joint analysis and interdisciplinary approach incorporating remote sensing and basic physics can help us better determine the landslide dynamics and mitigate the risks to humans.

1. Introduction

Landslides represent the downhill movement of detached earth materials on inclined surfaces. Specific terms for landslide systems are proposed according to different types of materials (e.g., soil and rock) and different modes of the movements (e.g., falls, topples, slides, lateral spreads, and flows) (Varnes, 1978). In particular, the slide-type landslides occur along a distinctive surface, usually the underlying firm bedrock. Debris slides are composed primarily of coarse materials including natural soils, unconsolidated sedimentary materials, and rock detritus. Increased pore (water) pressure or velocity can transition the sliding into the flowing mode of debris avalanches (Varnes, 1978). The viscosity is a fundamental rheological property to describe the dynamic or quasi-static flow-like behavior of the mobile masses, but it can vary by orders of magnitude depending on the composition, water content, and other environmental variables, as well as the applied methodology (van Asch et al., 2007). To improve our understanding of landslide constitutive properties, we focus on a type locality of slow-moving debris slides, the perennial moving Slumgullion landslide.

The Slumgullion landslide is a translational landslide in the San Juan Mountains in Hinsdale County, southwestern Colorado, USA. Nearly all movement occurs by sliding along bounding shear zones along a length of

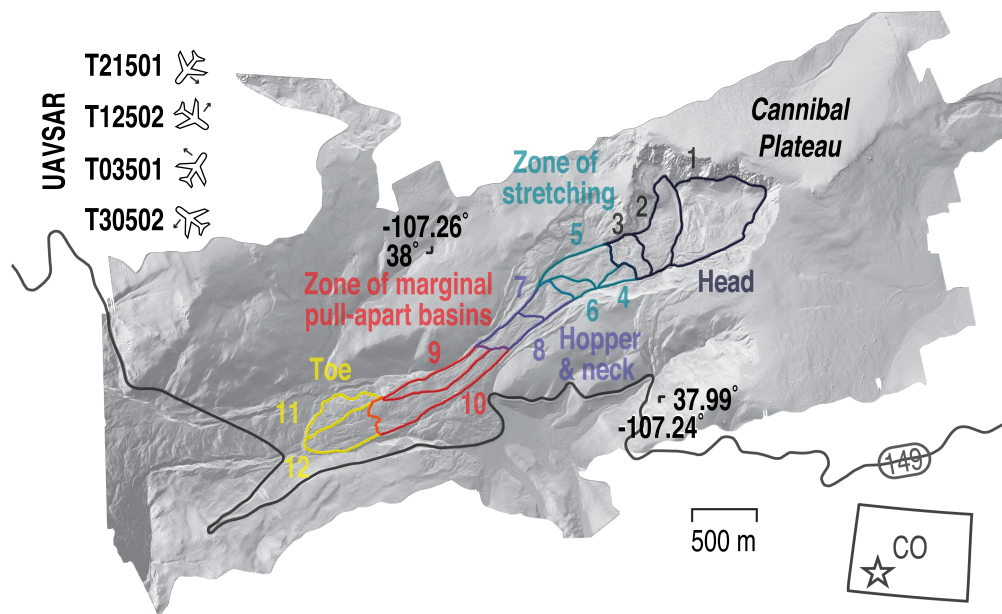


Figure 1. Shaded relief map of the Slumgullion landslide derived from a 0.5-m bare-earth LiDAR DEM obtained on 10 July 2015 (Lee, 2015). The orientation of UAVSAR flight lines and their respective range directions are shown in the top left. The gray line delineates Colorado State Highway 149. The star in the inset indicates the landslide location in Colorado, USA.

~4 km and an average width of 300 m, with a central neck section as narrow as ~200 m. The currently active landslide has been moving at an average rate of tens of millimeters per day for the past three centuries (e.g., Fleming et al., 1999; Schulz, Kean, & Wang, 2009; Schulz, Mckenna et al., 2009). These attributes make the Slumgullion an ideal natural laboratory for studying slow-moving landslides.

Abundant discontinuous landslide faults and secondary fractures developed and evolved during the landslide movement (Figure 1). Extensional features such as tension cracks and normal faults are exposed over the 1,300-m long and 700-m wide head zone. The zone of stretching, about 500 m in length and 300 m in width, is characterized by broad bands of tension cracks and normal faults. The narrowest 650-m long and 160-m wide hopper and neck zone resembles a funnel where the surfaces and trees tilt toward the central axis. Ponds present mostly in the lower parts of the landslide indicative of highly saturated conditions of the landslide mass. The 1,000-m long and 250-m wide releasing zone of marginal pull-apart basins, which were formed by stepped, subparallel strike-slip faults, widens gradually downhill. The 600-m long and 400-m wide emergent toe moves over the old, inactive landslide surface (Fleming et al., 1999). The toe is separated into two distinct parts (kinematic element #11 to the north and #12 to the south in Figure 1) with clearly separate movements, divided by a distinct right-lateral fault.

The landslide materials are of Tertiary volcanic origin from the Uncompahgre-San Juan caldera including tuffs and intrusive and extrusive rocks. The mineralogic composition is dominated by acid-sulfate hydrothermal alterations, including alunite, smectite, and opal (Chleborad et al., 1996), leading to a colorful mixture of yellow, white, gray, red, brown, and purple clays. Ring-shear tests on samples from Slumgullion suggest the soil cohesion and the angle of internal friction are about 23 kPa and 15.4°, respectively. The hydraulic conductivity ranges between 10^{-10} and 10^{-5} m/s, with an average of 4.2×10^{-10} m/s (Schulz, Mckenna, et al., 2009). The hydraulic diffusivity of its water-saturated materials is about 7.8×10^{-5} m²/s, a typical order-of-magnitude value for sandy to clayey soils (Schulz, Kean, & Wang, 2009).

Interferometric Synthetic Aperture Radar (InSAR) is a remote sensing approach to measure the regional ground displacement from the phase difference between SAR images collected at different times. InSAR has been widely used in a variety of geological hazards and processes such as landslides, earthquakes, volcanoes, aquifers, mining excavations, land subsidence, and nuclear explosions (e.g., Bürgmann et al., 2000; Handwerger et al., 2019; Hu et al., 2017, Hu et al., 2018; Kim et al., 2015; Lu & Dzurisin, 2014; Schaefer

et al., 2017; Shi, Lin, et al., 2019; Wang et al., 2011, 2018). Previous geodetic studies at the Slumgullion landslide focused on quantifying the magnitude of the movements and kinematics of landslide deformation (e.g., Coe et al., 2000; Coe et al., 2003; Delbridge et al., 2016; Fleming et al., 1999; Milillo et al., 2014; Schulz, Kean, & Wang, 2009; Schulz, Mckenna, et al., 2009; Schulz et al., 2017). Yet its rheology has not been well explored due to lack of knowledge to connect the geodetic observations and the physical properties; in addition, the resolution and coverage of geodetic data have been insufficient. For example, Milillo et al. (2014) used a total of 16 COSMO-SkyMed scenes to generate 1- and 4-day InSAR pairs between 2010 and 2013 and one set of 1-year-interval pixel offsets to capture the motions at the Slumgullion. They found that only the 1-day interferograms could be successfully unwrapped. Similarly, in our own analysis of Sentinel-1 data over Slumgullion, we found that only the slow-moving head and toe regions of the landslide can be studied due to extreme phase gradients in interferograms spanning ≥ 6 days (Hu, Bürgmann, Schulz, & Fielding, 2019). On the other hand, pixel offset analysis works well but at much reduced spatial resolution. Thus, satellite InSAR is generally not well suited for studying the detailed three-dimensional (3D) deformation of this landslide.

Thanks to the Uninhabited Aerial Vehicle SAR (UAVSAR) deployment at the Slumgullion, which includes a total of 124 scenes from four independent flight lines during 2011–2018, we are able to achieve one order of magnitude larger data quantity for a complete 3D high-resolution displacement map during a longer time span. Accurate measurements of 3D landslide movements are useful to infer the underlying rheological properties. Spatial displacement details also elucidate local variations in magnitude and orientation of the landslide deformation. Here, we present a new approach to quantifying the material viscosity of the non-Newtonian flow properties of the Slumgullion landslide.

2. Data and Methods

2.1. Airborne UAVSAR and LiDAR Data

UAVSAR is an airborne SAR system deployed by NASA/JPL, relying on an L-band (wavelength, ~ 0.238 m) sensor to observe the Slumgullion landslide. The azimuth and range pixel spacings are as small as 0.6 and 1.67 m, respectively. One to three campaigns were flown every year between April and November, during times of no/less snow cover. Each campaign collected two or three acquisitions along every flight line within a couple of weeks. Owing to the flexibility of airborne trajectories, the four independent flight lines have distinct imaging geometries (Figure 1). The T21501 and T03501 flight lines are almost parallel to the southwesterly slip direction and orthogonal to the T12502 and T30502 flight lines. Each flight line has about 30 scenes acquired between 2011 and 2018 (Table S1 in the supporting information).

The UAVSAR data are freely accessible (<https://uavstar.jpl.nasa.gov/cgi-bin/data.pl>) as single look complex stacks that can be used to generate the interferograms directly through conjugate multiplication. The phase is recorded as modulo of 2π cycles, and one fringe cycle corresponds to a radar line-of-sight motion of one half of the wavelength. To translate the interferogram into displacement measurements, we need to unwrap the fringes referenced to a stable area and multiply the phase-change values (in radians) by a coefficient related to the radar wavelength. For the phase unwrapping and displacement representation in our study, we assigned an off-slide area close to the middle part of the landslide as the reference area (yellow star in Figure 2).

To obtain an accurate estimate of the thickness of the landslide, we require a high-quality digital representation of the surface elevation of the Slumgullion. LiDAR DEM data acquisition (10 July 2015) and processing were completed by the National Center for Airborne Laser Mapping. In our study, we relied on the 0.5-m bare-earth LiDAR DEM product obtained from OpenTopography (Lee, 2015).

2.2. Bingham Plastic Model

The clay-rich deposits of the Slumgullion have medium to high plasticity (Chleborad et al., 1996). Insignificant shear deformation down to about 10-m depth found at a borehole inclinometer supports a finite plastic yield stress (Hu, Bürgmann, Schulz, & Fielding, 2019; Parise et al., 2003). The landslide is appropriately described as a viscoplastic debris slide (Cruden & Varnes, 1996; Schulz et al., 2017). Here, we consider the commonly used Bingham plastic model, which characterizes the deformation as a rigid body at low stresses but flows as a viscous fluid at high stress levels, to study the rheology at the gently inclined frontal toe of the landslide. The bottom layer above the underlying bedrock behaves like a fluid when the shear

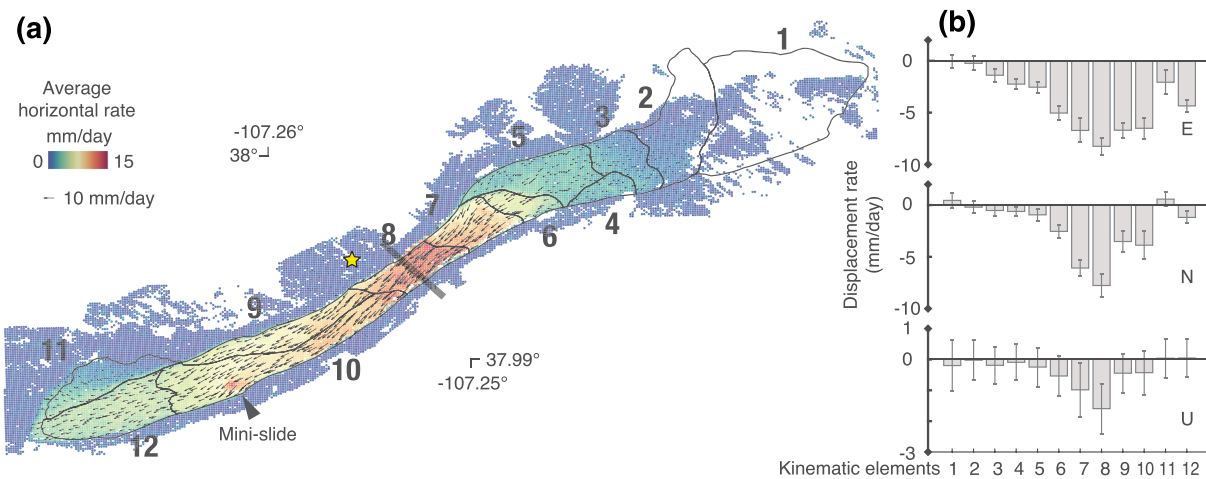


Figure 2. Landslide velocity map. (a) Map of the horizontal displacement rates. The arrows point in the slip directions. The length of the arrows and the colors represent the magnitude of the horizontal rates. The yellow star shows the reference in an off-slide area that the derived motions are relative to. The cross-sectional profile across the neck is used for the subsequent analysis. (b) The average displacement rates in east, north, and up directions for 12 kinematic elements from the head to the toe.

stress exceeds the yield stress and obeys $\tau = \tau_0 + \mu\dot{\gamma}$, where τ_0 is the yield stress at the yield interface $z = h_0$ (as illustrated by the Cartesian coordinate system on the slope in the inset of Figure 4), μ is the effective viscosity, and $\dot{\gamma}$ is the shear strain rate. On the other hand, the top layer translates as a rigid plug where $\tau \leq \tau_0$ (Bird et al., 1983).

The mass and momentum balance laws govern the flow behavior, supplemented by a no-slip condition on the bed, i.e., downslope velocity $u = 0$ at the base $z = H$; no shear stress at the free surface, i.e., $\tau = 0$ at $z = h$; and no shear above the yield surface, i.e., $\frac{\partial u}{\partial z} = 0$ at $z \geq h_0$. The stress depends on z and can be represented by (e.g., Mei & Yuhi, 2001),

$$\tau = \rho g(h - z) \left(\sin \theta - \cos \theta \frac{\partial h}{\partial x} \right). \quad (1)$$

The stress on the plane bed is given by

$$\tau_b = \rho g(h - H) \left(\sin \theta - \cos \theta \frac{\partial h}{\partial x} \right). \quad (2)$$

Following the Bingham flow theory, appreciable movements only occur when the bed stress is numerically larger than the yield stress. The longitudinal velocity beneath and above the yield surface h_0 is given by

$$u_x = \begin{cases} \frac{\rho g}{2\mu} \left(\sin \theta - \cos \theta \frac{\partial h}{\partial x} \right) [(h_0 - H)^2 - (z - h_0)^2] & \text{when } H < z \leq h_0 \\ \frac{\rho g}{2\mu} \left(\sin \theta - \cos \theta \frac{\partial h}{\partial x} \right) (h_0 - H)^2 & \text{when } h_0 < z \leq h \end{cases}. \quad (3)$$

Assuming that the transverse velocity vanishes everywhere, i.e., $u_y \equiv 0$, the local discharge q_x is an integration of the longitudinal velocity through depth.

$$q_x = \int_{H=0}^{h_0} u dz + u_p(h - h_0) = \frac{\rho g}{6\mu} \left(\sin \theta - \cos \theta \frac{\partial h}{\partial x} \right) h_0^2 (3h - h_0). \quad (4)$$

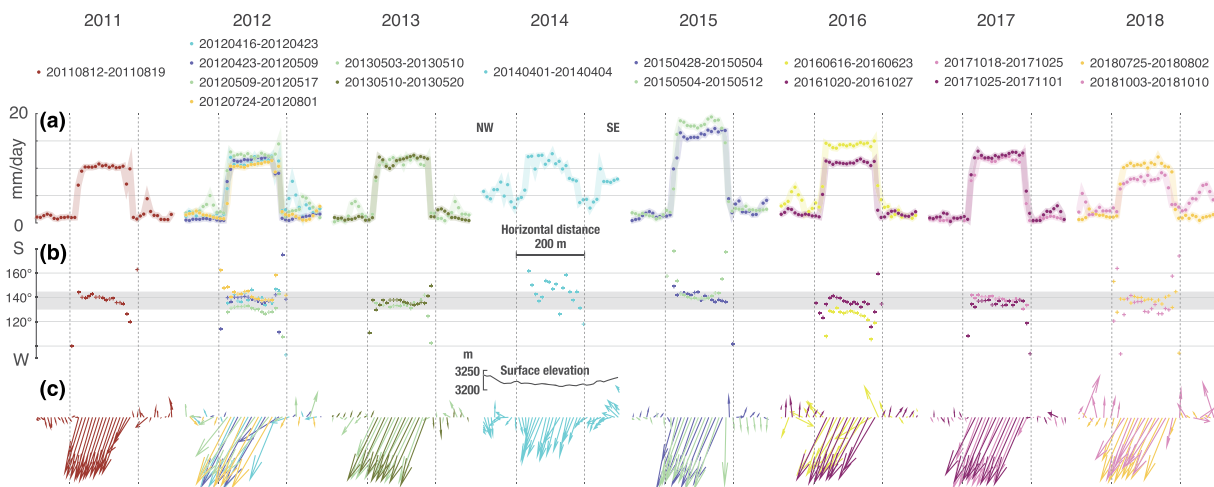


Figure 3. Time-variable horizontal rates and orientations crossing the landslide neck from northwest to southeast. Profile location is shown in Figure 2a. Dashed vertical lines denote the lateral boundaries. (a) Daily averaged horizontal rates. Points are sampled every 10 m, superimposed by light-colored fitting lines. (b) Slip vector orientations counterclockwise from the north, ranging from 90° (west) to 180° (south). Gray bar shows orientation of bounding faults along the neck (135° – 140°). (c) Plan view of the slip vectors.

3. Displacement Behaviors in Space, Time, and Orientation

The vertical motion is small and has a low signal-to-noise ratio; we thus focus on the horizontal component. The horizontal velocity vectors converge at the narrowest neck section with the largest slip rates in all three dimensions. The horizontal vectors spread out in the widening channel close to the toe (Figure 2a). The upper part of the landslide moves the slowest, followed by the toe. The northern part of the toe moves northwesterly, distinct from the mainly southwestward motions, while its west component is about half of the rate of the adjacent southern part of the toe (Figure 2b).

Slow-moving landslides are usually hydrologically driven (e.g., Cohen-Waeber et al., 2018; Hu et al., 2016; Hu, Bürgmann, Lu et al., 2019; Iverson et al., 2000; Scheingross et al., 2013; Shi et al., 2019), consistent with seasonal variations in landslide speed validated by GPS and extensometer observations at the Slumgullion (Coe et al., 2000; Coe et al., 2003; Schulz, Kean, & Wang, 2009; Schulz, Kean, & Wang, 2009). To compare the temporal behavior of the landslide system in further detail, we extract a profile crossing the ~200-m wide landslide neck across the fastest kinematic element 8 (location shown in Figure 2a). Landslide horizontal surface velocities increase abruptly close to the lateral margins and stay similar within the margins (Figure 3). Due to the limited observing years, irregular acquisition months, and variable annual precipitation, comparisons by stacking the monthly measurements can be biased. Instead, we arrange the landslide speeds for individual years (Figure 3). Overall, the monthly rates are the highest in May or June during abundant snow melt. Comparing different years, we notice that water year 2015 (WY2015) exhibits an especially high rate for April to June, whereas WY2018 has an especially low rate for October. The high slip rates in 2015 are consistent with its unusually high annual precipitation; whereas the slowest landslide motions in 2018 reflect a historic drought year (ref: <https://www.wcc.nrcs.usda.gov>).

Southwesterly slip orientations become focused within the margins but exhibit resolvable variability likely due to basal-surface irregularity and rheological heterogeneity. Increased southerly components compared to other parts of the slide occur at the neck (Figure 2a), where slip orientations vary between 130° and 145° counterclockwise from the north (gray horizontal bar in Figure 3b) while the bounding margins are oriented $\sim 138^\circ$. Displacements in the northwestern half are oriented more to the south than the southeastern half, apparently suggesting an internal horizontal rotation over the short distance.

4. Kinematics and Mechanics at the Advancing Toe

The classic Bingham model establishes a quantitative relationship between the longitudinal velocity and the viscosity of the mobilized materials if the density, slope, and thickness of the moving mass are known. We

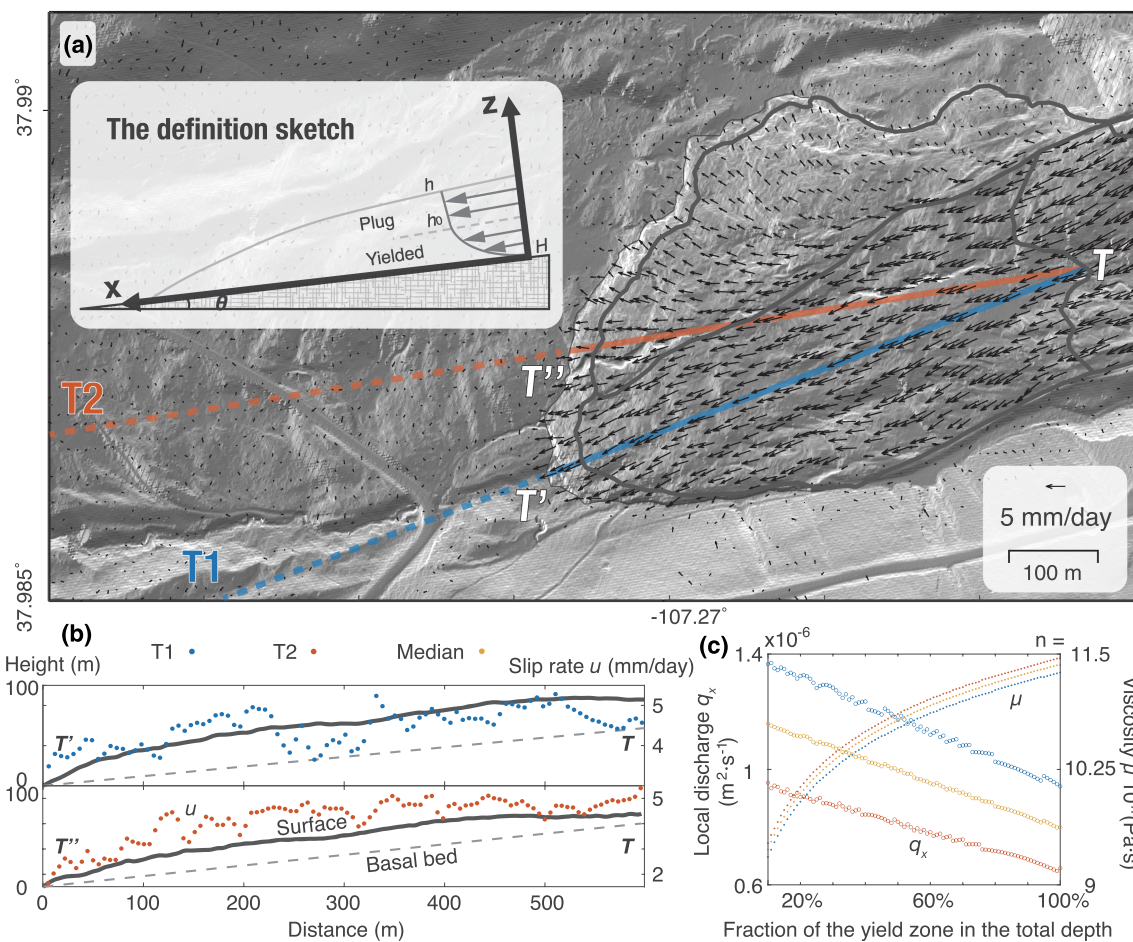


Figure 4. Kinematics and mechanics at the landslide toe. (a) Horizontal movement vectors. Gray thick lines show the margins for the active landslide and kinematic elements (Fleming et al., 1999; Guzzi & Parise, 1992; Parise & Guzzi, 1992). Gray thin line outlines the landslide margins determined by the morphologic features from the shaded-relief map of LiDAR DEM (Lee, 2015). Blue and orange lines show the positions of profiles T1 and T2 with consistent aspect directions, where the solid and dashed segments are on and off the slide, respectively. Inset illustrates the definition sketch for the Bingham model where x points downhill and z is oriented perpendicular to the inclined basal plane. (b) The longitudinal displacement rates (in colored dots), the landslide heights at the surface and basal beds referring to the zero-height toe tip (intersect between the solid and dashed profile lines). (c) Best-fit results on the viscosity and local discharge at the given fraction (10–100%) of the total depth to the yield zone. Blue and orange symbols represent the results of profiles T1 and T2, and yellow symbols are their average.

are able to quantify these parameters in the lower ~600-m long toe section of the Slumgullion. The landslide materials are mainly composed of fine-grained materials that exhibit plastic and viscoplastic behavior (e.g., Keefer & Johnson, 1983; Varnes & Savage, 1996). The slide is mostly saturated, and the average density of the saturated samples at the Slumgullion is $\sim 1.47 \times 10^3$ kg/m³ (Schulz, Kean, & Wang, 2009). The slope angle can be readily obtained from the LiDAR DEM. As the landslide is advancing by overriding the downhill terrain, we can estimate its thickness along the distal sections of the landslide by assuming the basal plane continues along the downhill topographic slope. Here, we rely on two longitudinal profiles T1 and T2 with slope aspects pointing in a consistent direction (Figure 4a). We project the off-slide surface upslope underneath the active surface and consider the difference in height to be the landslide thickness. Figure S1 shows the entire ~1,800-m profiles of the surface and basal elevations as well as the observed surface displacement rates, and Figure 4b focuses on the on-slide segment.

As we do not know where the yield surface is located, we consider a series of fractions, from 10% to 100%, of the total thickness below which yielding occurs. We then fit the displacement rates and viscosity based on Bingham flow theory (equation 3), assuming homogeneous landslide materials. The slope angle,

thickness, height gradient, and longitudinal slip rates for profiles T1 and T2 are 6.63° , 26.95 m, 0.11, and 4.5 mm/day and 5.98° , 19.25 m, 0.10, and 4.4 mm/day, respectively, where we take the median values of the on-slide profile segments for the latter three parameters. To match the displacement rates at the ground surface (assumed to be the same as rates at the yield surface at the base of the plastic plug), the best-fit solution gives rise to a viscosity on the order of 10^9 – $10^{11.5}$ Pa·s. Correspondingly, the depth-integrated local discharge given in equation 4) is estimated to be on the order of 0.6 – 1.4×10^{-6} m²/s (Figure 4c). The viscosity increases with an increasing fraction of the yield zone, whereas an opposing relationship exists for the local discharge.

A major uncertainty of this model comes from the input of depth estimates. Although the slope projection method has been suggested to be the most reliable method to extract the depth at the Slumgullion (Schulz, Kean, & Wang, 2009), a minor change in the slope angles can easily alter the thickness by several meters. The projection method is probably only appropriated for a small distance from the toe tip uphill as the slope is more likely to change at a greater distance and the basal bed of the landslide can be irregular (Coe et al., 2009; Delbridge et al., 2016; Hu, Bürgmann, Schulz, & Fielding, 2019).

Soil materials have a wide range of viscosity ranging from 10^{-3} to 10^{12} Pa·s (e.g., Lee & Widjaja, 2013; Ranalli et al., 2010; van Asch et al., 2007). Interest in viscosity in the landslide community has mostly focused on faster moving debris flow for which the lower values in this range are found to be appropriate. Some estimates are from lab experiments such as strain-controlled ring shear tests on isolated, limited representative samples. However, large uncertainties can result from slight variations in the condition of temperature, pressure, water content, methodology, etc. Also, the viscosity measured in the lab proved to be 10 to 1,000 times lower than the viscosity obtained from back analysis on the velocities measured at the surface or shallow depth from field instruments (equation 3) (van Asch et al., 2007). This may be because the negative pore pressure developed in a wavy slip surface and the convergent flow effects in natural landslide environments produce the velocity lower than the expectation in the lab (van Asch et al., 2007). Our estimates rely on the Bingham model using InSAR-measured rates and topography-inferred depths of the landslide toe in the intact, natural environment, and our viscosity estimates are numerically of a similar order as the modeled results on other landslides using their respective field velocities, for example, the Alverà mudslide in the Northern Alps in Italy (~ 0.1 mm/day; 10^{11} – 10^{12} Pa·s) (Ranalli et al., 2010), the La Valette landslide (5–260 mm/day; 1.2×10^{10} Pa·s), the La Mure landslide (5–260 mm/day; 9.0×10^9 Pa·s), and the Hau landslide (5–200 mm/day; 1.2×10^8 Pa·s) in French pre-Alps (van Asch et al., 2007). The determination of the intrinsic viscosity from the remotely sensed landslide deformation and morphology via the Bingham model is practical and effective.

5. Concluding Remarks

High-resolution UAVSAR data paired with the LiDAR DEM are especially valuable for a better understanding of the rheology of debris slides from remotely sensed surface displacements and topography (e.g., Finnegan et al., 2019). The surface displacements from UAVSAR InSAR reveal that the highest rates occur at the narrowest segment in the longitudinal middle part of the landslide during abundant snowmelt around May over the Slumgullion landslide. During the observing period from 2011 to 2018, the overall landslide speed is the largest in wet year 2015 and the slowest in the historic drought year 2018. Slip orientations can differ by about 10° over short latitudinal distances of 200 m and also change with time. To quantify the rheological properties of the slowly moving Slumgullion, we apply the Bingham flow model to simulate the non-Newtonian viscoplastic flow and compare the rates with InSAR observations. We focus on the frontal toe where the depth estimated from variation in topography and the surface slip rate of ~ 4.5 mm/day constrain the viscosity (10^9 – $10^{11.5}$ Pa·s) and local discharge (0.6 – 1.4×10^{-6} m²/s) under different degrees of plasticity. Our study proves that a joint analysis of remote sensing data can enhance our knowledge of the surface processes and the subsurface properties.

References

- Bird, R. B., Dai, G. C., & Yarusso, B. J. (1983). The rheology and flow of viscoplastic materials. *Reviews in Chemical Engineering*, 1, 1–70.
Bürgmann, R., Rosen, P. A., & Fielding, E. J. (2000). Synthetic aperture radar interferometry to measure Earth's surface topography and its deformation. *Annual Review of Earth and Planetary Sciences*, 28, 169–209. <https://doi.org/10.1146/annurev.earth.28.1.169>

Acknowledgments

This research was sponsored by the NASA Earth Surface and Interior Focus Area. We thank Editor Lucy Flesch and the anonymous reviewer for helpful comments. We thank the UAVSAR flight and data processing teams for providing the single look complex stacks (<https://uavstar.jpl.nasa.gov>). LiDAR DEM can be downloaded from the OpenTopography (<https://opentopography.org>). LiDAR data acquisition and processing completed by the NSF-funded National Center for Airborne Laser Mapping (NCALM). NCALM funding provided by NSF's Division of Earth Sciences, Instrumentation and Facilities Program. Mention of trade names or commercial products is not an endorsement or recommendation for use by the U.S. Government.

- Chleborad, A. F., Diehl, S. F., & Cannon, S. H. (1996). Geotechnical properties of selected materials from the Slumgullion landslide. In D. J. Varnes & W. Z. Savage (Eds.), *The Slumgullion Earth Flow: A Large-Scale Natural Laboratory* (Vol. 2130, pp. 67–71). U.S. Geol. Surv.
- Bull, Coe, J. A., Ellis, W. L., Godt, J. W., Savage, W. Z., Savage, J. E., Michael, J. A., et al. (2003). Seasonal movement of the Slumgullion landslide determined from Global Positioning System surveys and field instrumentation, July 1998–March 2002. *Engineering Geology*, 68(1–2), 67–101. [https://doi.org/10.1016/S0013-7952\(02\)00199-0](https://doi.org/10.1016/S0013-7952(02)00199-0)
- Coe, J. A., Godt, J. W., Ellis, W. L., Savage, W. Z., Savage, J. E., Powers, P. S., et al. (2000). Preliminary interpretation of seasonal movement of the Slumgullion landslide as determined from GPS observations. U.S. Geological Survey Open-File Report 00102.
- Coe, J. A., McKenna, J. P., Godt, J. W., & Baum, R. L. (2009). Basal-topographic control of stationary ponds on a continuously moving landslide. *Earth Surface Processes Landforms*, 34(2), 264–279. <https://doi.org/10.1002/esp.1721>
- Cohen-Waeber, J., Bürgmann, R., Chaussard, E., Giannico, C., & Ferretti, A. (2018). Spatiotemporal patterns of precipitation-modulated landslide deformation from independent component analysis of InSAR time series. *Geophysical Research Letters*, 45, 1878–1887. <https://doi.org/10.1002/2017GL075950>
- Cruden, D. M., & Varnes, D. J. (1996). Landslide types and processes. In A. K. Turner, & R. L. Schuster (Eds.), *Landslides, investigation and mitigation, transportation research board special report 247* (pp. 36–75). Washington, DC: National Research Council.
- Delbridge, B. G., Bürgmann, R., Fielding, E. J., Hensley, S., & Schulz, W. H. (2016). 3D surface deformation derived from airborne interferometric UAVSAR: Application to the Slumgullion landslide. *Journal of Geophysical Research: Solid Earth*, 121, 3951–3977. <https://doi.org/10.1002/2015JB012559>
- Finnegan, N. J., Broady, K. N., Nereson, A. L., Roering, J. J., Handwerger, A. L., & Bennett, G. (2019). River channel width controls blocking by slow-moving landslides in California's Franciscan mélange. *Earth Surface Dynamics*, 7, 879–894. <https://doi.org/10.5194/esurf-7-879-2019>
- Fleming, R. W., Baum, R. L., & Giardino, M. (1999). Map and description of the active part of the Slumgullion landslide, Hinsdale County, Colorado. U.S. Geological Survey Geologic Investigations Series Map I-2672
- Guzzi, R., & Parise, M. (1992). Surface features and kinematics of the Slumgullion landslide near Lake City, Colorado. U.S. Geological Survey Open-File Report 92-252, 45 p.
- Handwerger, A. L., Fielding, E. J., Huang, M. H., Bennett, G. L., Liang, C., & Schulz, W. H. (2019). Widespread initiation, reactivation, and acceleration of landslides in the northern California Coast Ranges due to extreme rainfall. *Journal of Geophysical Research: Earth Surface*, 124, 1782–1797. <https://doi.org/10.1029/2019JF005035>
- Hu, X., Bürgmann, R., Lu, Z., Handwerger, A. L., Wang, T., & Miao, R. (2019). Mobility, thickness, and hydraulic diffusivity of the slow-moving Monroe landslide in California revealed by L-band satellite radar interferometry. *Journal of Geophysical Research: Solid Earth*, 124. <https://doi.org/10.1029/2019JB017560>
- Hu, X., Bürgmann, R., Schulz, W. H., & Fielding, E. J. (2019) (December 9). Surface and subsurface dynamics of a perennial slow-moving landslide from ground, air and space. Under review in *Nature Communications*. <https://doi.org/10.31223/osf.io/vpj7b> (preprint at EarthArXiv)
- Hu, X., Lu, Z., Pierson, T. C., Kramer, R., & George, D. L. (2018). Combining InSAR and GPS to determine transient movement and thickness of a seasonally active low-gradient translational landslide. *Geophysical Research Letters*, 45, 1453–1462. <https://doi.org/10.1002/2017GL076623>
- Hu, X., Oommen, T., Lu, Z., Wang, T., & Kim, J. W. (2017). Consolidation settlement of Salt Lake County tailings impoundment revealed by time-series InSAR observations from multiple radar satellites. *Remote Sensing of Environment*, 202, 199–209. <https://doi.org/10.1016/j.rse.2017.05.023>
- Hu, X., Wang, T., Pierson, T. C., Lu, Z., Kim, J. W., & Cecere, T. H. (2016). Detecting seasonal landslide movement within the Cascade landslide complex (Washington) using time-series SAR imagery. *Remote Sensing of Environment*, 187, 49–61. <https://doi.org/10.1016/j.rse.2016.10.006>
- Iverson, R. M., Reid, M. E., Iverson, N. R., LaHusen, R. G., Logan, M., Mann, J. E., & Brien, D. L. (2000). Acute sensitivity of landslide rates to initial soil porosity. *Science*, 290(5491), 513–516. <https://doi.org/10.1126/science.290.5491.513>
- Keeler, D., & Johnson, A. (1983). Earth flows: Morphology, mobilization, and movement. U.S. Geol. Surv. Prof. Pap., 126.
- Kim, J. W., Lu, Z., Qu, F., & Hu, X. (2015). Pre-2014 mudslides at Oso revealed by InSAR and multi-source DEM analysis. *Geomatics, Natural Hazards and Risk*, 6(3), 184–194. <https://doi.org/10.1080/19475705.2015.1016556>
- Lee, H. (2015). Slumgullion landslide, Colorado airborne lidar survey. National Center for Airborne Laser Mapping (NCALM), distributed by OpenTopography. <https://doi.org/10.5069/G91834KD>
- Lee, S. H. H., & Widjaja, B. (2013). Phase concept for mudflow based on the influence of viscosity. *Soils and Foundations*, 53(1), 77–90.
- Lu, Z., & Dzurisin, D. (2014). *InSAR imaging of Aleutian volcanoes: Monitoring a volcanic arc from space*. Springer Praxis Books, Geophysical Sciences, ISBN 978-3-642-00347-9 (p. 390). New York: Springer. <https://doi.org/10.1007/978-3-642-00348-6>
- Mei, C. C., & Yushi, M. (2001). Slow flow of a Bingham fluid in a shallow channel of finite width. *Journal of Fluid Mechanics*, 431, 135–159.
- Milillo, P., Fielding, E. J., Shulz, W. H., Delbridge, B. G., & Bürgmann, R. (2014). COSMO-SkyMed spotlight interferometry over rural areas: The Slumgullion landslide in Colorado, USA. *IEEE Journal of Selected Topics in Applied Earth Observations and Remote Sensing*, 7(7), 2919–2926. <https://doi.org/10.1109/JSTARS.2014.2345664>
- Parise, M., Coe, J., Savage, W., & Varnes, D. J. (2003). The Slumgullion landslide (southwestern Colorado, USA): Investigation and monitoring. International workshop “Occurrence and mechanisms of flow-like landslides in natural slopes and earthfills”.
- Parise, M., & Guzzi, R. (1992). Volume and shape of the active and inactive parts of the Slumgullion landslide, Hinsdale County, Colorado. U.S. Geological Survey Open-File Report, 92-216, p. 29.
- Ranalli, M., Gottardi, G., & Medina-Cetina, Z. (2010). Uncertainty quantification in the calibration of a dynamic viscoplastic model of slow slope movements. *Landslides*, 7, 31–41. <https://doi.org/10.1007/s10346-009-0185-0>
- Schaefer, L. N., Wang, T., Escobar-Wolf, R., Oommen, T., Lu, Z., Kim, J., et al. (2017). Three-dimensional displacements of a large volcano flank movement during the May 2010 eruptions at Pacaya Volcano, Guatemala. *Geophysical Research Letters*, 44, 135–142. <https://doi.org/10.1002/2016GL071402>
- Scheingross, J. S., Minchew, B. M., Mackey, B. H., Simons, M., Lamb, M. P., & Hensley, S. (2013). Fault-zone controls on the spatial distribution of slow-moving landslides. *GSA Bulletin*, 125(3–4), 473–489.
- Schulz, W. H., Coe, J. A., Ricci, P. P., Smoczyk, G. M., Shurtliff, B. L., & Panosky, J. (2017). Landslide kinematics and their potential controls from hourly to decadal timescales: Insights from integrating ground-based InSAR measurements with structural maps and long-term monitoring data. *Geomorphology*, 285, 121–136. <https://doi.org/10.1016/j.geomorph.2017.02.011>
- Schulz, W. H., Kean, J. W., & Wang, G. (2009). Landslide movement in Southwest Colorado triggered by atmospheric tides. *Nature Geoscience*, 2(12), 863–866. <https://doi.org/10.1038/ngeo659>

- Schulz, W. H., Mckenna, J. P., Kibler, J. D., & Biavati, G. (2009). Relations between hydrology and velocity of a continuously moving landslide—Evidence of pore-pressure feedback regulating landslide motion? *Landslides*, 6(3), 181–190. <https://doi.org/10.1007/s10346-009-0157-4>
- Shi, G., Lin, H., Bürgmann, R., Ma, P., Wang, J., & Liu, Y. (2019). Early soil consolidation from magnetic extensometers and full resolution SAR interferometry over highly decorrelated reclaimed lands. *Remote Sensing of Environment*, 231, 111–231. <https://doi.org/10.1016/j.rse.2019.111231>
- Shi, X., Yang, C., Zhang, L., Jiang, H., Liao, M., Zhang, L., & Liu, X. (2019). Mapping and characterizing displacements of active loess slopes along the upstream Yellow River with multi-temporal InSAR datasets. *Science Total Environment*, 674, 200–210. <https://doi.org/10.1016/j.scitotenv.2019.04.140>
- van Asch, T. W. J., Van Beek, L. P. H., & Bogaard, T. A. (2007). Problems in predicting the mobility of slow-moving landslides. *Engineering Geology*, 91(1), 46–55.
- Varnes, D. J. (1978). Slope movement types and processes, in Schuster, R. L., and Krizek, R. J., eds., *Landslides—Analysis and control*: National Research Council, Washington, D. C., Transportation Research Board, Special Report 176, p. 11–33.
- Varnes, D. J., & Savage, W. Z. (Eds.) (1996). The Slumgullion earth flow: A large-scale natural laboratory. U.S. Geol. Surv. Bull., 2130, p. 95.
- Wang, T., Perissin, D., Rocca, F., & Liao, M. (2011). Three Gorges Dam stability monitoring with time-series InSAR image analysis. *China Earth Sciences*, 54(5), 720–732. <https://doi.org/10.1007/s11430-010-4101-1>
- Wang, T., Shi, Q., Nikkhoo, M., Wei, S., Barbot, S., Dreger, D., et al. (2018). The rise, collapse, and compaction of Mt. Mantap from the 3 September 2017 North Korean nuclear test. *Science*, eaar7230. <https://doi.org/10.1126/science.aar7230>